

## Analysis of a capped carbon nanotube by linear-scaling density-functional theory

C J Edgcombe\*, J Whaley-Baldwin, S M Masur and C H W Barnes

TFM Group, Department of Physics, University of Cambridge, CB3 0HE, Cambridge, UK

\*corresponding author, email [cje1@cam.ac.uk](mailto:cje1@cam.ac.uk)

### Abstract

The apex region of a capped (5,5) carbon nanotube (CNT) has been modelled with the DFT package ONETEP, using boundary conditions provided by a classical calculation with a conducting surface in place of the CNT. The DFT solution also provides details of the individual orbitals for the CNT tip, their physical distribution and their occupation, allowing the work function to be estimated. Application of an external electric field produces very little change in the charge distribution on the CNT, but extends the HOMO near the emission threshold. In this case, the classical image potential appears to overestimate the lowering of barrier height produced by exchange and correlation effects.

### Keywords

Carbon nanotube, density functional theory, Wannier functions, charge density, density of states, Fermi level, HOMO

### 1. Introduction

The challenge of describing field-emitting structures and field emission continues to be addressed by development of methods of analysis. All these methods preserve the concept of tunnelling through a classically-forbidden region that provided one of the first successes of wave mechanics [1]. However, many further details of the emission process have proved difficult to describe simply, while estimation of practical parameters such as the emitting area remains a challenge for both experimental and theoretical technique. Recent developments in microscopy, such as near-field scanning electron microscopy [2], have increased the need for methods that can describe the distribution of emitted current in detail. The widely-known semi-analytic theory uses some classical modelling, with known limitations. However, density functional theory (DFT) can describe some behaviour from first principles with more accuracy, over a limited volume. In 2002, Han and Ihm presented a study with Lee of a time-dependent (5,5) carbon nanotube (CNT) [3], and another study of a (10,10) CNT [4]. Zheng et al [5] divided the length of a SWCNT into subranges, iterating by solving each subrange in turn with DFT while the others were simulated by molecular mechanics. Csányi et al [6] introduced the use of non-planar basis functions (as outlined below) and provision of the exterior boundary conditions for the DFT solution from an equivalent classical calculation. Wang, Shao and Li [7] applied multi-scale DFT to model edges of graphene and open-ended CNTs, and Li [8] extended the method to project the current distribution to a screen.

Here we outline the program ONETEP [9], which is a linear-scaling code based on time-independent DFT, and give a survey of its results for a capped single-walled carbon nanotube (SWCNT). The initial motivation was that the use of plane waves as basis functions, as found in many DFT packages, is undesirable for non-periodic systems of hundreds of atoms or more. The number of plane waves and the solution time needed to model the system accurately would both be very large. As an

---

<https://doi.org/10.1016/j.ultramic.2018.11.007>

© <2018>. This manuscript version is made available under the CC-BY-NC-ND 4.0 license

<http://creativecommons.org/licenses/by-nc-nd/4.0/>

alternative, ONETEP (Order-N Electronic Total Energy Package) [9] uses a basis with which the solution time scales only as the number of electrons in the model. The method is usable at present only with external fields below the threshold for current flow, yet it has yielded a rich seam of data. Results outlined here, obtained both with zero external field and with applied field below threshold, include the spatial distribution of charge density, orbital energies at non-zero temperatures, distribution of the highest occupied molecular orbital (the HOMO), distribution of total potential and potential due to non-classical effects ( $E_{xc}$ ), and total and local densities of states. The calculated  $E_{xc}$  is compared with the classical image potential for the SWCNT.

## 2 Density functional theory

The formulation of DFT by Kohn and Sham [10] describes the total state of a system by minimising a sum of energy terms of the form

$$E[n] = \sum_i \langle \psi_i | -\frac{1}{2} \nabla^2 | \psi_i \rangle + E_{ext}[n] + E_{Coul}[n] + E_{xc}[n]$$

where the first term on the right represents the kinetic energy of a non-interacting set of orbitals, the second term is the energy due to the externally applied field, the third term is the energy due to classical Coulomb repulsion and the fourth term estimates the energy due to all non-classical effects. This last term includes effects of exchange and correlation, which are partially modelled by the image potential. Here  $n(\mathbf{r})$  is the density of electrons in the system. The  $\psi_i$  are Kohn-Sham orbitals, artificial states for single particles that are obtained by solving a Schrödinger-like equation with an effective potential which is related to the exact potential. If the orbitals were obtained from the exact potential, the work function would be the negative of the potential of the HOMO, relative to the vacuum level. However, the exact potential is usually not available, and the energies of Kohn-Sham HOMOs are known to agree only moderately well with other estimates of work function for CNTs [11]. Detailed studies ([12], [13]) have discussed suitable forms to obtain better estimates of the orbital energies.

In ONETEP,  $n(\mathbf{r})$  is defined as a sum of quadratic terms that are obtained from a kernel matrix and Wannier functions  $\phi_\alpha(\mathbf{r})$ . The solution method varies both the kernel coefficients and the Wannier functions adaptively. As a result, the solution time scales linearly with the number of orbitals  $N$ , which equals the number of electrons in the system. For problems with  $N$  of the order of hundreds, this property offers a great benefit relative to other methods whose solution time is proportional to  $N^3$  or more. The number of Kohn-Sham orbitals equals the number of electrons, so in the absence of applied field half these orbitals are occupied, with two electrons of opposite spins per orbital.

ONETEP was extended in 2005 [6] to provide solutions when the given conditions include both a non-periodic potential distribution on the boundary of the volume to be analysed (the 'DFT box') and the excess electronic charge induced within the box (as found in the macroscopic system). When the applied external field is below the emission threshold, the result describes an equilibrium ground state. The results outlined here show many more details of the atomic system than are available from classical approximations and assumptions. However, the orbitals computed here are not complex but real, so they do not model emission of current or show variation of phase with azimuth.

The quantities that can be reported by ONETEP include charge density, potential energy, local density of states (LDoS) and spatial distribution of individual orbitals. These are reported at points on a regular cubic grid. In addition, the energy and occupation of orbitals are reported. Calculations at non-zero temperatures are made by the ensemble-DFT method [14]. The program assumes the

Fermi-Dirac distribution, so at temperatures high enough to produce some occupancy values between 0 and 1, the apparent Fermi level (relative to vacuum) can be found graphically (see Section 4.2.1). At lower temperatures, the apparent level can be estimated from the mean of HOMO and LUMO (lowest unoccupied) levels. In this paper we quote energies relative to the Fermi level deduced in this way, with the warning that energy differences from this level may be underestimated [11].

### 3. Method of calculation

To obtain a solution within acceptable computing time, we define a limited volume (the DFT box) over which the density functional calculation will be solved. The volume used in the present work was a cube of side 5 nanometres. Values were calculated at points on a cubic grid of side 12 picometres. Using the program Virtual Nanolab [15], we built a single-walled cylindrical (5,5) tube of carbon atoms, one end of which was capped with half a  $C_{60}$  molecule (having a pentagon on its axis). The combination of tube and hemisphere contained 150 carbon atoms and was terminated at the uncapped end with 10 hydrogen atoms. The atomic positions were optimised until the force on each

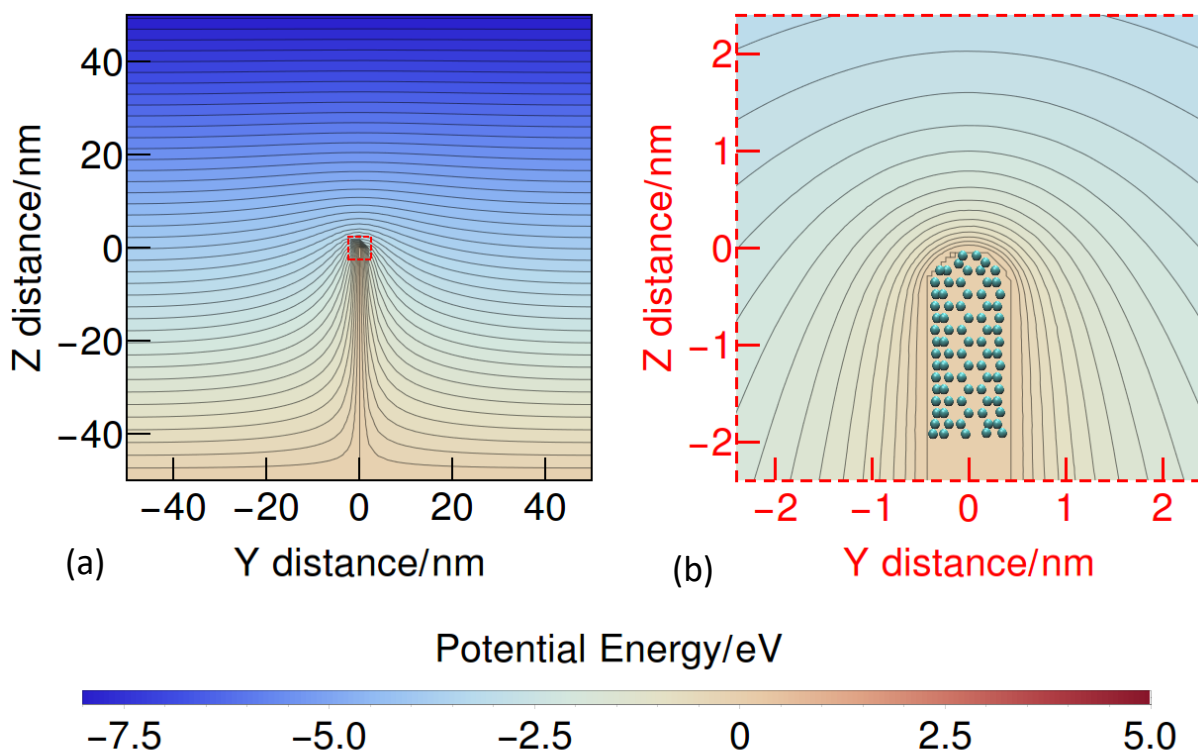


Fig. 1. Geometry analysed: (a) CNT supported on planar cathode electrode at  $z = -50$  nm, with parallel anode plane at  $z = +50$  nm. The small red box around the CNT tip defines the volume shown in (b); (b) the final 1.8 nm of the capped (cylindrical) CNT, in the (cubic) DFT box of side 5 nm. The equipotentials at intervals of 0.2 V are from the classical solution for a conductor with the diameter of the Fermi equipotential for the CNT, with an anode-cathode voltage of 8 V.

atom was less than  $0.05$  eV/Å. In the optimised CNT, the carbon cores are at a radius of  $0.317$  nm from the axis and form a structure  $1.83$  nm long (Fig. 1(b)).

To solve the system with an applied electric field, we used a combination of classical and DFT calculations. The system for classical calculation consisted of parallel cathode and anode planes of diameter  $100$  nm and separated by  $100$  nm, with the CNT of total length  $50.3$  nm standing

perpendicular to and in contact with the cathode plane (Fig. 1(a)). As the (5,5) CNT is known to be a conductor, it was modelled by a conducting rod with a hemispherical end and diameter 0.864 nm, chosen to approximate that of the Fermi equipotential (as discussed in Section 5.2). The voltage distribution over the surface of the DFT box was found using the solver FlexPDE [16] and interpolated onto the mesh for the DFT box. The potential found by the classical calculation corresponds to the classical energy ( $E - E_{xc}$ ) in the DFT system, where  $E$  is the total energy and  $E_{xc}$  is the non-classical contribution. Although in the classical model the field is zero in the body of the rod, the DFT calculation solves for the varying potential distribution through the CNT.

Applying an external field induces additional charge onto the CNT. In the classical model, with the CNT connected to the cathode plane, the charge induced within the defined DFT box is a fixed multiple of the anode-cathode voltage. For the DFT calculation, in contrast, the short section of the CNT within the box is not connected to any electrode, so the charge on it can be varied independently and this also varies its mean potential relative to the boundary (by Gauss' theorem). The system to be analysed by DFT thus differs from the macroscopic system, because it requires the induced charge to be specified, in addition to the boundary potential. This charge can be found (again using Gauss' theorem) by integrating the classical normal electric field over the surface of the box. Thus to provide initial conditions for the DFT calculation, both the boundary potential and the excess charge in the box are needed, and so the distributions of both voltage and normal electric field over the surface of the DFT box are extracted from the classical solution.

The DFT calculation reported here used the LDA functional with the CAPZ parameterization. It produces potentials relative to the vacuum potential, which is well defined when the external field is zero. For non-zero applied fields the potential reference is less clear. We can however use the rule known for semiconducting systems, that the macroscopically measurable voltage of an electrode corresponds to the Fermi level for that electrode. We assume the CNT to be in a simple circuit with cathode and anode as described above, in which the voltage of the cathode and CNT is held fixed as the anode-cathode voltage is varied. Then the Fermi level of the CNT remains constant as the external field varies. Thus, provided we can identify the Fermi levels for different applied fields, we can compare the potential distributions around the tip by aligning their Fermi levels. When this is done, the potential distribution near the atomic cores is found to vary very little with applied field.

## **4. Results for capped (5,5) SWCNT**

### ***4.1 Classical solution with applied field***

The first non-zero anode voltage used was 8V relative to the cathode, corresponding to a background field (in the absence of the nanotube) of 0.08 V/nm. The resulting equipotentials for this system are shown in Fig. 1(a). Fig. 1(b) shows a section through the volume of the DFT box, with classical equipotentials for voltages greater than the cathode voltage of 0V and with the equilibrium structure of the carbon cores superimposed.

### ***4.2 DFT solution for charge density***

The electron density distribution found by DFT with zero applied field is shown in Fig. 2. Isosurfaces are plotted for densities of 0.02%, 0.25% and 1% of the global maximum density ( $704 \text{ e}/\text{\AA}^3$  at zero field). Most of the charge is localised near the carbon cores, but there is also a continuous sheath of relatively low density at a slightly greater distance from the cores. This continuous sheath provides a conducting path for charge to move along and around the CNT surface, up to a density between 0.25% and 1% of the global maximum.

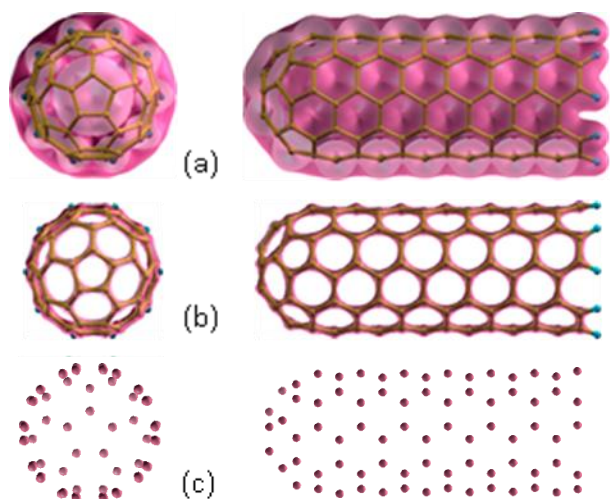


Fig. 2. Electron density isosurfaces for zero applied field (those with 0.08 V/nm applied field are identical in appearance at this scale). The isosurfaces are at (a) 0.02%, (b) 0.25%, (c) 1.00% of the global maximum charge density ( $\approx 0.14, 1.8, 7.0 \text{ e}\text{\AA}^{-3}$  respectively). In (a) and (b), isosurfaces are in purple with the atomic frame of the CNT added. The views on the left are from the cap end.

The background field of  $0.08 \text{ Vnm}^{-1}$  was chosen to induce exactly 2 additional electrons into the DFT box. The corresponding change of charge density is shown in Fig. 3. The magnitude of the change in density shown by these isosurfaces is  $2.5 \times 10^{-3} \text{ e}\text{\AA}^{-3}$ , which is about  $1.4 \times 10^{-3}$  of the static charge density of the middle surface in Fig. 2.

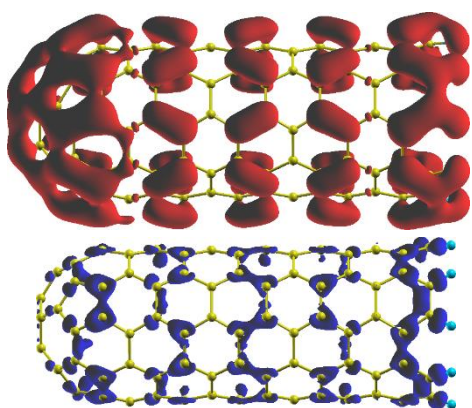


Fig 3. Change in electron density on application of  $0.08 \text{ Vnm}^{-1}$  with 2 added electrons. The red isosurface shows where the electron density has increased by  $2.5 \times 10^{-3} \text{ e}\text{\AA}^{-3}$  and the blue isosurface shows where the density has decreased by  $2.5 \times 10^{-3} \text{ e}\text{\AA}^{-3}$ , relative to zero-field values.

#### 4.3 The Fermi-Dirac distribution and Fermi level relative to vacuum

The number of orbitals calculated by ONETEP equals the number of electrons defined in the DFT box. In zero field, half of these orbitals are occupied by electrons of both spins. The modelling in ONETEP assumes the Fermi-Dirac distribution, and the probability of occupation of each orbital (the 'occupancy') may take values between 0 and 1. At temperatures high enough for the occupancies near the Fermi level to differ appreciably from 0 or 1, the Fermi level relative to vacuum can be found graphically with apparently high precision, though it is known that estimates of work function made from this result may be underestimates. Table 1 lists, and Fig. 4 plots, energy levels for some orbitals near the HOMO in zero external field, at a temperature of 1000K. With zero applied field, the mid-gap value of energy is estimated to be about  $-4.42 \text{ eV}$  relative to vacuum level. The levels in Table 1 show some pairing. At lower temperatures, the Fermi level can be estimated as the mean of HOMO and LUMO energies. Since the number of orbitals equals the number of electrons in the DFT box, the number to be expected for the full length of the CNT is very much greater than those reported here, with a correspondingly smaller spacing between the energies of orbitals.

Table 1. Orbitals near HOMO at 1000K.

Orbital	Energy /eV	Occupancy
310	-3.315728	0.000002700
309	-3.662847	0.000147200
308	-3.664395	0.000149900
307	-3.924569	0.003097400
306	-3.993173	0.006863900
305	-4.870496	0.994560200
304	-4.880958	0.995181300
303	-5.529966	0.999997400

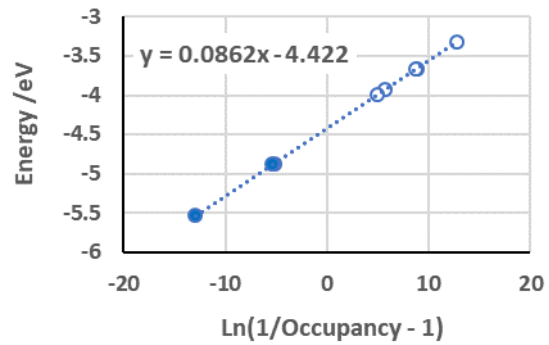


Fig. 4. Plot to show Fermi-Dirac distribution at 1000K in zero field.

#### 4.4 Local density of states (LDoS)

The LDoS for the 4 planes perpendicular to the CNT axis and closest to the end cap has been plotted for three applied fields. Applying a field produces small changes in the pattern but the general form remains similar. The general pattern, relative to the Fermi level, moves with applied field, but the apparent movement depends on whether the Fermi level used is always that for zero field or as determined for each applied field. The behaviour relative to the Fermi level for each applied field is shown in Fig. 5. The LDoS moves by 0.50 eV for applied field of 0.08 V/nm and by 0.84 eV for 0.16 V/nm.

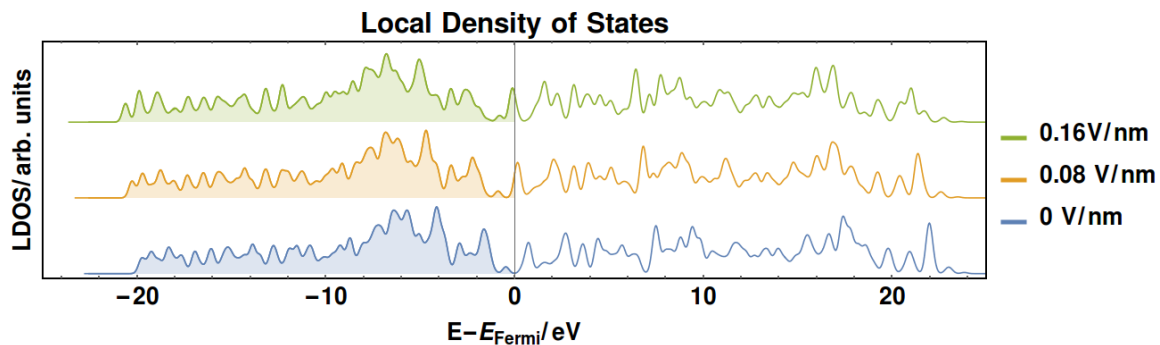


Fig. 5 Local density of states as a function of energy relative to Fermi level for 3 values of applied field. The density has been collected from the 4 planes perpendicular to the axis and closest to the end cap. The displacement of the whole LDoS distribution, relative to the Fermi level, by the field is 0.50 eV for applied field of 0.08 V/nm and 0.84 eV for 0.16 V/nm.

#### 4.5 Spatial distribution of the HOMO

Fig. 6 shows isosurfaces for one amplitude (+ and -) of the HOMOs found with three external fields. For larger amplitudes, the distribution appears discontinuous, like the charge density in Fig. 2(c). The three fields used for these plots induce different numbers of electrons into the DFT box. Hence the HOMOs have progressively higher orbital numbers as the field increases. The distribution on the CNT surface thus changes with the applied field.

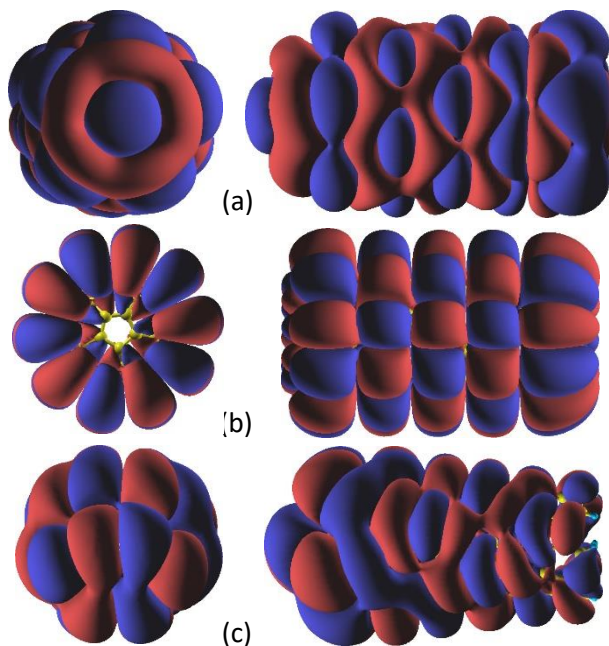


Fig. 6 HOMO isosurfaces at amplitude of  $0.0004 \text{ (eA}^{-3})^{1/2}$ , with Kohn-Sham orbital number  $n_{KS}$ : (a) in zero field,  $n_{KS} = 305$ ; (b) in  $0.08 \text{ Vm}^{-1}$ ,  $n_{KS} = 306$ ; (c) in  $0.16 \text{ Vm}^{-1}$ ,  $n_{KS} = 307$ .

#### 4.6 Potential with applied field

A longitudinal section through the DFT box, with equipotentials resulting from an applied anode-cathode voltage of 8V, is shown in Fig. 7. The distribution of potential near the hemispherical cap

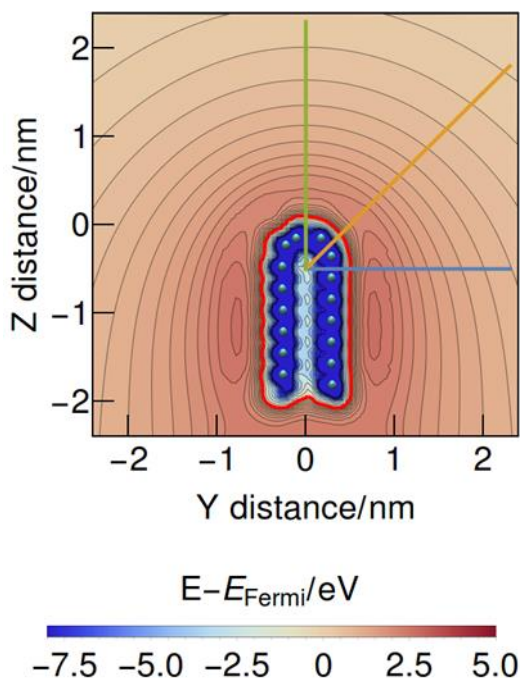


Fig. 7. Section containing the CNT axis, showing the total potential distribution  $E$  around the CNT tip with a background field of  $0.08 \text{ Vnm}^{-1}$  and with 2 excess electrons. The red outline is the Fermi equipotential ( $E_F$ ). Equipotentials above and below  $E_F$  are at intervals of  $0.2 \text{ eV}$  and  $1 \text{ eV}$  respectively. The coloured lines starting from the point ( $z = -0.5 \text{ nm}$ ,  $y = 0$ ) indicate the directions (green =  $0^\circ$ , orange =  $45^\circ$  and blue =  $90^\circ$  relative to the axis) used for the potential plots of Fig. 8. The dots indicate the positions of carbon cores.

and cylindrical surface is much smoother than that of charge density, which is reasonable since the potential is a double integral of the charge density, in accordance with Poisson's equation. The boundary potentials differ from the classical boundary of Fig. 1(b), because Fig. 7 shows the total potential including  $E_{xc}$  which creates the potential barrier. The applied field was lower than the threshold value for emission and, at this low field, no indication has been seen of field penetration at the apex. The radius of the Fermi equipotential from the axis is  $0.470 \text{ nm}$  in zero field, and  $0.489 \text{ nm}$  in the background field of  $0.08 \text{ Vnm}^{-1}$ .

The potential distribution (including  $E_{xc}$ ) along the straight lines in Fig. 7 from the point ( $z = -0.5\text{nm}$ ,  $r = 0$ ),  $0.1\text{nm}$  below the centre of the hemispherical cap, is shown in Fig. 8, relative to the Fermi level, for three directions relative to the axis and three values of background field: zero,  $0.08$  and  $0.16\text{ Vnm}^{-1}$ . For the conditions modelled in Fig. 8, it appears that a small increase in applied voltage above  $16\text{V}$  would reduce the maximum potential on axis (plot (a)) to below the Fermi level, so causing strong emission.

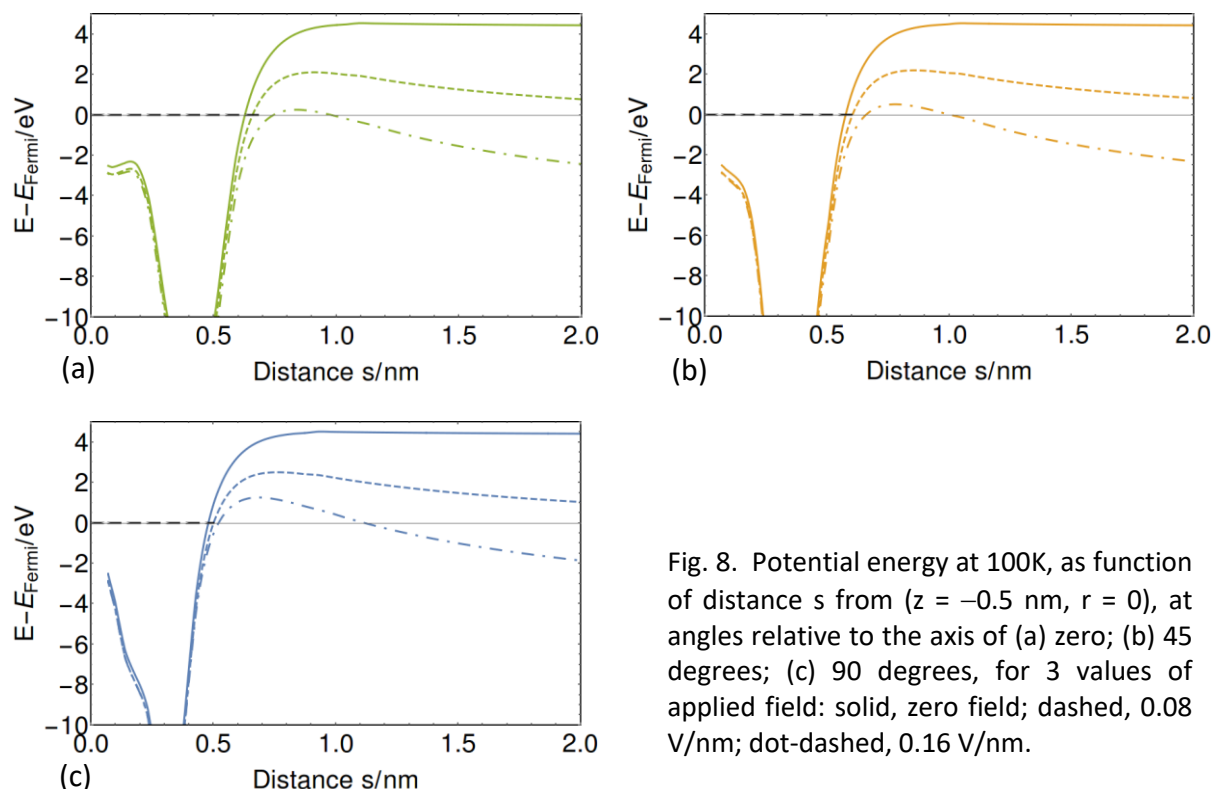


Fig. 8. Potential energy at  $100\text{K}$ , as function of distance  $s$  from ( $z = -0.5\text{ nm}$ ,  $r = 0$ ), at angles relative to the axis of (a) zero; (b)  $45$  degrees; (c)  $90$  degrees, for 3 values of applied field: solid, zero field; dashed,  $0.08\text{ V/nm}$ ; dot-dashed,  $0.16\text{ V/nm}$ .

Fig. 9 shows more detail of the potentials ( $E - E_{xc}$ ) and  $E$ , on the axis. The potential variation near the core is not exact but is approximated by a pseudopotential, as is usual in DFT. The classical part of the potential ( $E - E_{xc}$ ) shows a drop of a few eV in the core region, but the contribution from  $E_{xc}$

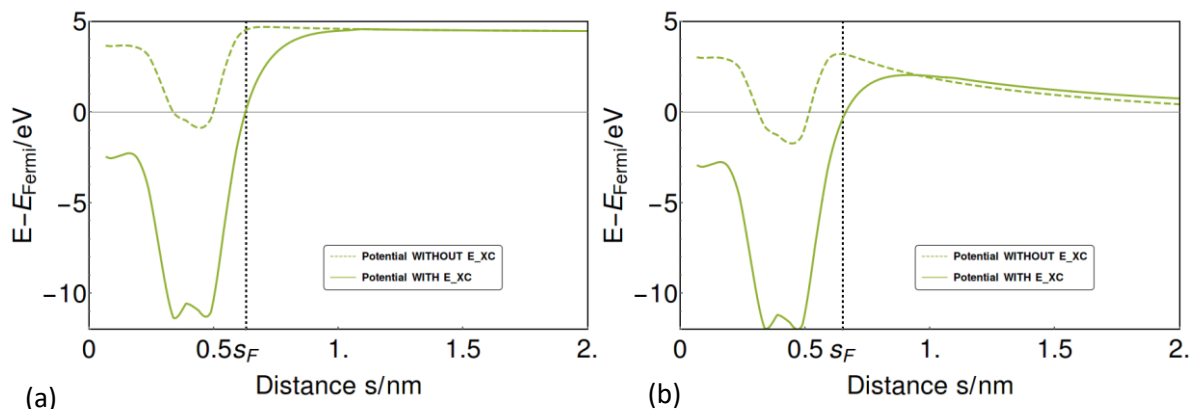


Fig. 9 Potential energy at  $100\text{K}$  as function of distance along axis from ( $z = -0.5\text{nm}$ ,  $r = 0$ ) for (a) zero applied field and (b) applied field of  $0.08\text{ V/nm}$ . Each plot shows 2 curves from a single calculation which included exchange and correlation effects. One curve is the total energy  $E$  including  $E_{xc}$ , the other is the classical component ( $E - E_{xc}$ ).

produces a much greater drop in potential over the regions around the cores. The classical image potential approximates the part of  $E_{XC}$  that is further from the core than the Fermi equipotential, as discussed in Section 5.3.

## 5. Discussion

The following remarks apply to the system modelled here, but not necessarily to other configurations of field emitters. It will be convenient to denote by  $s_F$  the intersection of the axis with the Fermi equipotential of  $E$ , at zero external field, as shown at  $s = 0.63$  nm in Fig. 9(a).

### 5.1 Charge density

Fig. 2 shows that much of the electron density is localised around the carbon cores, but there is also a continuous sheath of lower density that allows conduction over all the CNT surface. Any external electric field induces charge on this outer sheath. This screens the cores so that they are not much affected by the external field, as shown by the plots of potential in the core regions of Fig. 9.

### 5.2 The equivalent classical surface

As suggested in Section 3 above, consistency between the classical and atomic models requires agreement as to what outline in the atomic model should be taken as ‘the surface’ of the equivalent classical conductor. As, in classical terms, the surface of a conductor is an equipotential, it should agree with an equipotential in the atomic model. Where details are available at atomic scale, an obvious possibility is to define the classical surface as the equipotential for the Fermi level at zero external field, as shown in Fig. 9 at  $s_F$ . When field is applied, the Fermi equipotential moves away from  $s_F$  and electrons are also able to move further from the cores.

### 5.3 Comparison of exchange and image potentials

$E_{XC}$  as calculated by ONETEP is plotted as a function of axial distance in Fig. 10, for zero applied field and at 100K. The classical image potentials for a planar and a spherical conductor are also shown. For an image calculation, there is the question of where to locate the conducting surface that provides an electrostatic mirror. Fig. 2(a) and (c) show that charge is not continuous between the cores, but a continuous layer of charge exists at the Fermi equipotential. We therefore choose the Fermi equipotential as the notional mirror surface for an image calculation, and approximate it by a plane or by a spherical surface with the local radius of the Fermi equipotential at the axis. These approximating surfaces meet the axis at  $s_F$ , as defined in Sec. 5.2 and shown on Fig. 10.

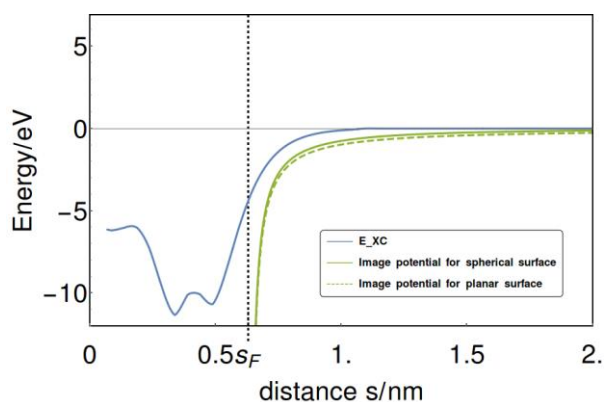


Fig. 10. Exchange and correlation energy ( $E_{XC}$ ), as a function of distance along the axis. The cores are nearest to the axis at  $s = 0.42$  nm. The potential in the cores was simulated by a pseudopotential. Image potentials are also shown, for a plane conductor and for a spherical one with the radius of the Fermi equipotential, both meeting the axis at  $s_F$ .

Fig. 9(a) shows that the classical potential ( $E - E_{XC}$ ) rises to just over the vacuum level at  $s_F$ , so in zero external field the change of the total  $E$  as  $s$  increases from  $s_F$  to infinity is due almost entirely to  $E_{XC}$ . Fig 9(b) shows that the combination of an external field and  $E_{XC}$  causes the barrier height to be lower

than it would be with external field alone, as shown also by Fig. 8. The equivalent effect, with an image potential in place of  $E_{xc}$ , is well known in classical estimates of barrier transmission. In Fig. 10, for  $s > s_F$ ,  $E_{xc}$  is more positive than the image potentials. So the classical image potentials seem likely, in this case, to overestimate the lowering of barrier height when field is applied.

## 6. Conclusions

Modelling of the properties of a capped (5,5) CNT by DFT using localizable functions has given detailed estimates of the atomic properties that are not available from classical approximations. The available outputs include (a) the spatial distribution of charge density, showing a low-density sheath which enables conduction and screens the core potential from external fields; (b) the distribution and relative energies of individual orbitals including the HOMO; (c) the local density of states; (d) the distribution of total potential and also the estimated component due to exchange and correlation effects ( $E_{xc}$ ). Results can be compared for zero external field and for applied fields that are below the threshold for electron emission. These results are obtained by use of the linear-scaling DFT program ONETEP over the apex region of the CNT, with boundary conditions set by classical modelling of the macroscopic system.

Results by this method show that in the core region  $E_{xc}$  is as large as 10 eV or more for the structure considered. The charge density around the cores is contained within the equipotential at the Fermi level; this equipotential in zero external field appears to be a suitable definition of 'the surface' for classical modelling. Outside this equipotential, the distribution of potential is determined mainly by  $E_{xc}$ . The detailed calculation of  $E_{xc}$  suggests that the classical image potentials used hitherto may overestimate the contribution of exchange and correlation effects to reducing the barrier height in an external field.

The spatial distribution of the HOMO at zero or low field is somewhat similar to that of the electronic charge. Applying a field (below the emission threshold) induces extra charge onto the CNT but produces little change in its distribution. However, as the field increases, the orbital number of the Kohn-Sham HOMO changes, and near the emission threshold its amplitude develops a maximum at the apex.

## Acknowledgments

The authors thank Prof. M.C. Payne for the opportunity to use ONETEP, and Prof. C-K. Skylaris, Dr J Dziejic, Dr. G. Constantinescu and E. Liscott of the TCM Group of C.U. Department of Physics for their advice on running it.

Figures 1 and 7 were plotted using Mathematica [17]. Figures 2, 3 and 6 were plotted using XcrysDen [18].

The authors declare no conflicting interests. The research leading to these results has received funding from the People Programme (Marie Curie Actions) of the European Union's Seventh Framework Programme FP7/2007-2013/ under REA grant agreement n 606988.

## References

- [1] R.H. Fowler, L. Nordheim, Electron Emission in Intense Electric Fields, Proc. R. Soc. London Ser. A-Mathematical Phys. Sci. 119 (1928) 173–181. doi:10.1098/rspa.1928.0091.
- [2] D.A. Zanin, H. Cabrera, L.G. De Pietro, M. Pikulski, M. Goldmann, U. Ramsperger, D. Pescia, J.P. Xanthakis, Fundamental Aspects of Near-Field Emission Scanning Electron Microscopy, in: Adv. Imaging Electron Phys. Vol 170, 2012: p. 227.

- [3] S. Han, M.H. Lee, J. Ihm, Dynamical simulation of field emission in nanostructures, *Phys. Rev. B - Condens. Matter Mater. Phys.* 65 (2002) 085405. doi:10.1103/PhysRevB.65.085405.
- [4] S. Han, J. Ihm, First-principles study of field emission of carbon nanotubes, *Phys. Rev. B - Condens. Matter Mater. Phys.* 66 (2002) 241402. doi:10.1103/PhysRevB.66.241402.
- [5] X. Zheng, G.H. Chen, Z. Li, S. Deng, N. Xu, Quantum-Mechanical Investigation of Field-Emission Mechanism of a Micrometer-Long Single-Walled Carbon Nanotube, *Phys. Rev. Lett.* 92 (2004) 12–15. doi:10.1103/PhysRevLett.92.106803.
- [6] G. Csányi, C.-K. Skylaris, A. Nevidomskyy, C.J. Edgcombe, Ab initio approach to a lightning rod, (2005). <http://www.tcm.phy.cam.ac.uk/~ndd21/esdg.html> (accessed 5 Oct 2018).
- [7] W. Wang, J. Shao, Z. Li, The exchange–correlation potential correction to the vacuum potential barrier of graphene edge, *Chem. Phys. Lett.* 522 (2012) 83–85. doi:doi:10.1016/j.cplett.2011.12.002.
- [8] Z. Li, Density functional theory for field emission from carbon nano-structures, *Ultramicroscopy.* 159 (2015) 162–172. doi:10.1016/j.ultramic.2015.02.012.
- [9] C.-K. Skylaris, P.D. Haynes, A.A. Mostofi, M.C. Payne, Introducing ONETEP: Linear-scaling density functional simulations on parallel computers, *J Chem Phys.* 122 (2005) 084119. doi:10.1063/1.1839852.
- [10] W. Kohn, L.J. Sham, Self-Consistent Equations Including Exchange and Correlation Effects, *Phys. Rev.* 140 (1965) A1133–A1138.
- [11] R. Stowasser, R. Hoffmann, What Do the Kohn - Sham Orbitals and Eigenvalues Mean ?, *J. Am. Chem. Soc.* (1999) 3414–3420.
- [12] S. Hamel, P. Duffy, M.E. Casida, D.R. Salahub, Kohn – Sham orbitals and orbital energies : fictitious constructs but good approximations all the same, *J. Electron Spectrosc.* 123 (2002) 345–363.
- [13] T. Grabo, E.K.U. Gross, Density-functional theory using an optimized exchange-correlation potential, *Chem. Phys. Lett.* 240 (1995) 141–150.
- [14] N. Marzari, D. Vanderbilt, M.C. Payne, Ensemble density-functional theory for ab initio molecular dynamics of metals and finite-temperature insulators, *Phys. Rev. Lett.* 79 (1997) 1337–1340. doi:10.1103/PhysRevLett.79.1337.
- [15] J. Schneider, J. Hamaekers, S. Chill, S. Smidstrup, J. Bulin, R. Thesen, A. Blom, K. Stokbro, ATK-ForceField: a new generation molecular dynamics software package, *Model. Simul. Mater. Sci. Eng.* 25 (2017) 085007. doi:10.1088/1361-651X/aa8ff0.
- [16] PDE Solutions Inc, FlexPDE, (n.d.). <https://www.pdesolutions.com>.
- [17] Wolfram Research, Mathematica, (2018).
- [18] A. Kokalj, Computer graphics and graphical user interfaces as tools in simulations of matter at the atomic scale, *Comput. Mater. Sci.* 28 (2003) 155–168. doi:10.1016/S0927-0256(03)00104-6.